Chemical Papers (2023) 77:1181–1200
https://doi.org/10.1007/s11696-022-02513-5

ORIGINAL PAPER

Giant milkweed plant-based copper oxide nanoparticles for wound dressing application: physicochemical, bactericidal and cytocompatibility profiles

G Ambarasan Govindasamy[1,2] · Rabiatul Basria S. M. N. Mydin[1] · Nor Hazliana Harun[1,3] · Wan Nuramiera Faznie Wan Eddis Effendy[1] · Srimala Sreekantan[4]

Received: 28 July 2022 / Accepted: 20 September 2022 / Published online: 24 October 2022

Abstract

Present wound dressing materials have limitation in treating skin pathogens colonization associated with open wound infections. Recently, plant-based synthesis of inorganic oxide nanomaterials has received countless attention to tackle the mention limitation. This study investigated the physicochemical, bactericidal and cytocompatibility properties of copper oxide (CuO) nanoparticles from giant milkweed medicinal plant were produced at different calcination temperatures (i.e., 400 and 500 °C). Giant milkweed plant is scientifically known as *Calotropis gigantea* (*C. gigantea*). The oval-shaped CuO-500C exhibited improved bactericidal properties toward tested skin pathogens than CuO-400C. Successful green synthesis of CuO nanoparticles with the presence of bioderived elements was affirmed through both EDAX and XRD. Furthermore, FTIR and UV–visible analyses confirmed phenolic and carbonyl compounds. The MIC value for CuO-400C and CuO-500C toward the skin pathogens was ranging from 1.25 to 10 mg/mL and 0.3125 to 5 mg/mL, respectively. MBC value for CuO-400C and CuO-500C was 20 mg/mL and 2.5–20 mg/mL, respectively. From time-kill assay we found that *Staphylococcus aureus* (*S. aureus*) and *Escherichia coli* (*E. coli*) colonies began to decrease substantially after 6 h, and bactericidal activity was noticed at 12 h. However, the methicillin-resistant *Staphylococcus aureus* (MRSA) treated with CuO-500C was fully inhibited at 24 h. Besides, zone of inhibition of 10 mg/mL CuO-500C was greater than other samples. CuO-500C (2.5–10 mg/mL) had good cytocompatibility (> 90%) without any alteration on fibroblast cells morphology. Conclusively, CuO-500C nanoparticles demonstrated cytocompatibility potential with strong bactericidal properties for wound dressing material application.

✉ Rabiatul Basria S. M. N. Mydin
rabiatulbasria@usm.my

G Ambarasan Govindasamy
gambarasan@student.usm.my

Nor Hazliana Harun
hazlianarun@student.usm.my

Wan Nuramiera Faznie Wan Eddis Effendy
wan.amiera@student.usm.my

Srimala Sreekantan
srimala@usm.my

[1] Department of Biomedical Science, Advanced Medical and Dental Institute, Universiti Sains Malaysia, 13200 Bertam, Kepala Batas, Pulau Pinang, Malaysia

[2] Ann Joo Integrated Steel Sdn Bhd, Lot 1236, Prai Industrial Estate, 13600 Prai, Penang, Malaysia

[3] Neogenix Laboratoire Sdn Bhd, 12-3, Jalan Permas 10/6, Bandar Baru Permas Jaya, 81750 Masai, Johor, Malaysia

[4] School of Materials and Mineral Resources Engineering, Universiti Sains Malaysia, Engineering Campus, 14300 Nibong Tebal, Pulau Pinang, Malaysia

Graphical abstract

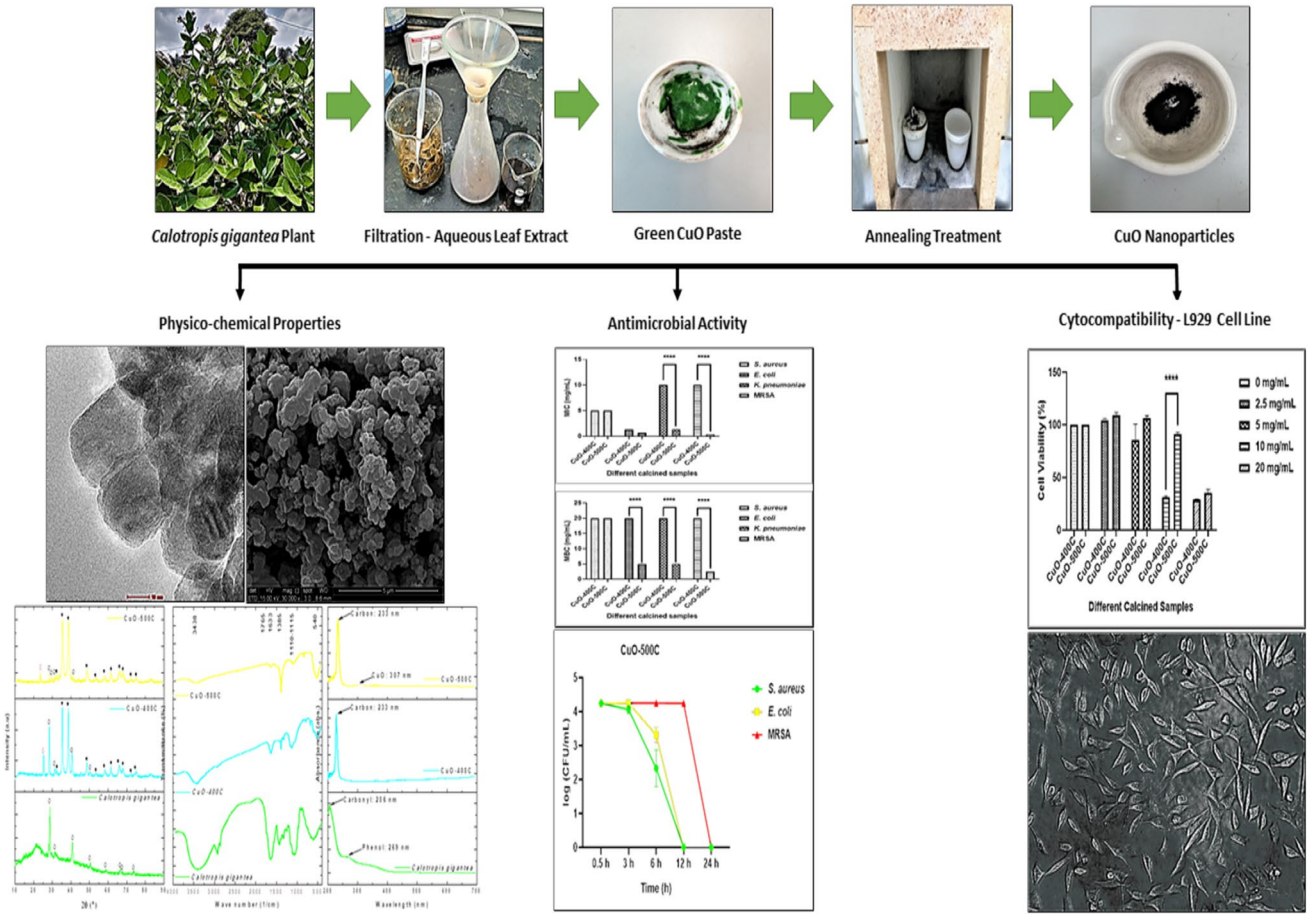

Keywords Giant milkweed · CuO nanoparticles · Wound dressing material · Skin pathogens · Bactericidal · Cytocompatibility

Abbreviations

C. gigantea	*Calotropis gigantea*
CuO	Copper oxide
ROS	Reactive oxygen species
SSA	Specific surface area
MIC	Minimum inhibitory concentration
MBC	Minimum bactericidal concentration
XRD	X-ray diffraction
MDR	Multi-drug resistant
E. coli	*Escherichia coli*
K. pneumoniae	*Klebsiella pneumoniae*
S. aureus	*Staphylococcus aureus*
MRSA	Methicillin-resistant *Staphylococcus aureus*
C	Carbon
Ca	Calcium

List of symbols

D	Crystallite size, nm
λ	X-ray wavelength of Cu Kα radiation, nm
θ	Bragg diffraction angle, °
T	Temperature, °C
T	Time, h

Introduction

Skin pathogens usually associated with open wound ulcers, such as surgical infections and wounds, diabetic infections and foot ulcers, pressure ulcers, arterial ulcers, chronic ulcers, skin disorders and infections, traumatic wounds and venous ulcers, are the most common wound injuries that lead to human morbidity and mortality, including amputation and

death (Nussbaum et al. 2018). Medicare cost estimates for the treatment of all wound types range from $28.1 billion to $96.8 billion, and the highest expenses are for surgical wounds, followed by diabetic foot ulcers (Nussbaum et al. 2018). Wounds infected by multidrug-resistant (MDR) and non-MDR skin pathogens are hardly treatable (Uckay et al. 2015; September et al. 2019; Wang et al. 2019). Broad-spectrum antibiotics, such as vancomycin, oxacillin, penicillin, cefoxitin and chloramphenicol, are ineffective to control the growth of MDR skin pathogens and are not preferred in colonized open wound ulcers (Hamzah et al. 2019). Besides, non-MDR Gram-positive *Staphylococcus aureus* is also one of the most common skin pathogens responsible for infectious wound ulcers (Wong et al. 2015). In past researchers found that, among 77 wound swab samples studied at Local Hospital, Malaysia, 82 isolates consist of Gram-negative (71.1%) and Gram-positive bacteria (27.7%) (Nur Hilda Hanina et al. 2015). Moreover, a recent study showed that roughly 23,000 deaths a year in the USA and more than 33,000 deaths in Europe are due to antibiotics failure in treating MDR strain-infected ulcers (Pacios et al. 2020).

Increasing antibiotic resistance has stimulated research on green-synthesized copper oxide (CuO) nanoparticles with different morphologies as a bactericidal agent to overcome open wound ulcers (Table 1). In this regard, many papers have reported the usage of different types of natural plant extract to synthesize desired properties of green-synthesized nanoparticles with excellent bactericidal properties (Akintelu et al. 2020; Thakur et al. 2019; Lediga et al. 2018; Mtambo et al. 2019). The rise of green-synthesized CuO in biomedical field can provide genuine support in facilitating the healing process of locally colonized open wound infections and repairing injured tissue. Currently, highly moisturized bactericidal dressings, including those that contain metals or metal oxide nanoparticles, are used locally to manage skin ulcer infection while accelerating wound healing (Janowska et al. 2019; Han and Ceilley, 2017; Djavid et al. 2020; Frykberg and Banks, 2015; Bogoslovskaya et al. 2022). These dressings help in accelerating the wound recovery process through the release of metal ions and the generation of reactive oxygen species (ROS) (Jadhav et al. 2017). In addition, calcination temperature predominantly affects the physicochemical (i.e., size and shape) as well as their bactericidal properties of metal and metal oxide nanoparticles (El Desouky et al. 2020; Yu et al. 2003; Saravanan and Sivasankar, 2016; Jiao et al. 2018; Azam et al. 2012).

Generally, low-temperature annealed green-synthesized nanoparticles were expected to have remarkable medicinal properties and exhibit steady and low ROS release which is safe and non-toxic against cell line (Umar et al. 2015; Azizi et al. 2016). Wider zone of inhibition against several skin pathogens and improved antioxidant activity was also captured for low-temperature annealed CuO nanoparticles than high-temperature calcined CuO nanoparticles (Hamid et al. 2021). Besides of that, the degree of crystallinity and clusters or boundaries of CuO grains size were further increased at extremely high annealing temperature between 600 and 900 °C (Luna et al. 2015; George et al. 2020). Larger grain size and crystallite size at high calcination temperature predominantly affect and weaken the antibacterial properties (Hamid et al. 2021). A similar phenomenon was also reported in previous research, where CuO nanoparticles crystallization was incomplete at very low temperature of 200 °C (Luna et al. 2015). As referred to Table 1, calcination temperature between 400 and 500 °C was most preferred in green synthesis of CuO nanoparticles. Furthermore, formation of pure Cu/Cu_2O/CuO nanoparticles was seen during slight changes on full width at half maximum (FWHM) peak intensity of XRD at calcination temperature between 400 and 500 °C (Fuku et al. 2020).

Therefore, the aims of this work were to synthesize green CuO nanoparticles with cytocompatibility properties using the aqueous extract of the giant milkweed medicinal plant and the effect of low calcinations temperature (400 and 500 °C) on the physicochemical and bactericidal properties of CuO was determined. The milky and evergreen flowering plant of giant milkweed is a genus from family of *Asclepiadaceae,* and the traditional use of this plant in treating open wound ulcers is well documented (Sharma et al. 2015). It is also known as "*Erukku"* and quite popular among *Konar* community of Tamil Nadu (Jayakumar et al. 2018). Additionally, the bioderived CuO was evaluated for bactericidal activities by employing skin-related pathogens using minimum inhibitory concentration (MIC), minimum bactericidal concentration (MBC), time-kill assay and Kirby-Bauer disc diffusion technique. At final stage, cytocompatibility assay was performed against green CuO on fibroblast cells lines model according to ISO 10993–5 (2009) guidelines.

Materials and methods

Materials and chemicals

Copper (II) nitrate trihydrate (99.5%) was purchased from Merck (Darmstadt, Germany). Dimethyl sulfoxide (DMSO) obtained from Sigma-Aldrich was used as diluents for samples preparation. Commercial CuO (< 10 µm) was used as commercial control purchased from Sigma-Aldrich. Luria–Bertani (LB) nutrient medium was purchased from Sigma-Aldrich (Darmstadt, Germany) and was used to culture non-MDR and MDR skin pathogens. Oxoid™ cefoxitin bactericidal susceptibility disk with concentration of 30 µg was introduced as an antibiotic positive control. The fibroblast cells lines model, L929 used in this work, was purchased from American Type Culture Collection (ATCC,

Table 1 Physicochemical, bactericidal and cytocompatibility properties of green-synthesized copper oxide (CuO) nanoparticles

Precursor	Reducing/capping agent	Calcination temperature °C	Size of NPs (nm)	Shape of NPs	Antimicrobial activity	Killing mechanism	Toxicity	Application	References
Cupric Nitrate	*Calotropis gigantea*	400 °C	20–30	Spherical	Nil	Nil	Nil	Dye-sensitized solar cells	(Sharma et al. 2015)
Copper (II) acetate monohydrate	*Oak Fruit Hull* (*Jaft*)	500 °C	Nil	Quasi-spherical	Nil	Nil	Nil	Photocatalytic	(Sorbiun et al. 2018)
Copper nitrate trihydrate	Banana Peel	400 °C	50–85	Spherical	Nil	Nil	Nil	Photocatalytic	(Aminuzzaman et al. 2017)
Copper sulfate dehydrate	*Ocimum basilicum*	Nil	70	Spherical	ZOI for *E. coli*: 9.8 mm and *S. aureus*: 7.2 mm	Copper ions	Nil	Food and medical	(Altikatoglu et al. 2017)
Cupric nitrate	*Gloriosa superba* L	400 °C	5–10	Spherical	ZOI at 1000 µg/100 µL: *K. aerogenes*: 15.67 mm, *P. desmolyticum*: 5.33 mm, E. *coli*: 13.67 mm and *S. aureus*: 6 mm	Copper ions	Nil	Antibacterial	(Naika et al.2015)
Copper (II) sulfate pentahydrate	*Malus Domestica*	Dried under lamp	18–20	Spherical	ZOI at 100 µg/ml: *E. coli*: 17 mm and *S. aureus*: 19 mm	Cu^{2+} ion release, electrostatic interaction and ROS generation	Nil	Biological agent	(Jadhav et al. 2017)
Copper nitrate	*Drypetes sepiaria*	Nil	~18	Nil	Nil	Nil	Nil	Photocatalytic	(Narasaiah et al. 2017)
Copper nitrate	*Catharanthus Roseus* Leaf Extract	400 °C	23	Nanorod	Nil	Nil	Nil	Catalytic material	(Maria et al. 2020)
Copper sulfate	*Phoenix dactylifera* L extract	400 °C	20–28	Spherical and irregular	Nil	Nil	Nil	Nil	(Berra et al. 2018)
Copper sulfate	*Callistemon viminalis Leaf Extract*	60 °C	423	Nil	At 1024 µg: ZOI for *E. coli*: 14 mm and *A. baumannii*: 12 mm	Nil	Nil	Nil	(Sharma et al. 2018)
Cu $(NO_3)_2.3H_2O$	*Tinospora crispa* leaves extract	450 °C	10–40	Spherical	Nil	Nil	Nil	Photocatalysts	(Apriandanu et al. 2019)

Table 1 (continued)

Precursor	Reducing/capping agent	Calcination temperature °C	Size of NPs (nm)	Shape of NPs	Antimicrobial activity	Killing mechanism	Toxicity	Application	References
$Cu(NO_3)_2.3H_2O$	*Abutilon indicum* leaf extract	400 °C	16.78	Spherical	*S. aureus, Klebsiella* and *B. subtilis* with ZOI of 10 mm, 14 mm and 15 mm	Copper ions	Nil	Photo-catalytic, antimicrobial and antioxidant	(Ijaz et al. 2017)
Copper sulfate	*Lemongrass* Leaf extract	Nil	5.67–9.10	Spherical	Nil	Nil	Nil	Photocatalysts	(Tu, 2019)
$CuSO_4.5H_2O$	*Momordica charantia* fruit extract	Nil	61.48	Nanorod	ZOI for *B. cereus*: 31.66 mm	Copper ions	Nil	Biomedical	(Qamar et al. 2020)
Copper acetate monohydrate	*Psidium guajava* leaf extract	400 °C	2–6	Spherical	Nil	Nil	Nil	Photocatalysts	(Singh et al. 2019)
Copper sulfate	*Adiantum lunulatum* whole plant extract	Nil	6.5	Spherical	Nil	Nil	Nil	Nil	(Sarkar et al. 2020)
Cupric nitrate	*Plectranthus amboinicus* leaves extract	450 °C	5–30	Spherical and circular	ZOI for *E. coli*: 13.65 mm, *K. pheumoniae*: 13.40 mm, *P. aeruginosa*: 13.05 mm, *S. aureus*: 13.25 mm, *S. phogenes*: 12.55 mm, and *B. Subtilis*: 12.80 mm	Cu^{2+}, OH^-radicals, O_2^{2-} ions and hydrogen peroxide (H_2O_2)	Nil	Drug	(Velsankar et al. 2020)
Hydrated copper chloride	*Saraca indica* Leaves	100 °C	40–70	Spherical	Nil	Nil	Nil	Fluorescence emitting materials	(Prasad et al. 2017)
Copper sulfate	*Cassia auriculata* leaf extract	Nil	23	Spherical	Nil	Nil	RAW 264.7 cell lines: low cytotoxicity up to 200 µg/mL	Drug delivery vehicle	(Shi et al. 2017)
Copper nitrate	*Juglans regia* leaf extract	300 to 500 °C	80	Spherical	MIC value of 1.78% w/v	Particles attachment	Nil	Medicine and food packaging	(Asemani et al. 2019)

Table 1 (continued)

Precursor	Reducing/capping agent	Calcination temperature °C	Size of NPs (nm)	Shape of NPs	Antimicrobial activity	Killing mechanism	Toxicity	Application	References
Copper sulfate	*Phyllanthus Amarus* leaf extract	Nil	20	Large aggregated particles	ZOI for *B. subtilis*: 31 mm, *S. aureus*: 28 mm, *E. coli*: 24 mm and *P. aeruginosa*: 25 mm	Amines and carboxyl groups	Nil	Nil	(Acharyulu et al. 2014)
Copper nitrate	*Aloe vera* leaf extract	Nil	20–30	Spherical	At 100 µg: ZOI for *A. hydrophila*: 22 mm, *P. Fluorescens*: 19 mm and *F. branchiophilum*: 17 mm	Copper ions	Nil	Antimicrobial agents	(Kumar et al. 2015)
Copper chloride salt	*Calotropis gigantea* floral extract	Nil	25–35	Spherical	Nil	Nil	Zebrafish embryos: 50% viability rate for 50 mg/l	Nil	(Kumari et al. 2017)
Copper sulfate	*Convolvulus percicus* L. leaves	400 °C	15–30	Spherical	MIC for *S. aureus*: 1.56 and *E. coli*: 6.25 µg/ml	ROS generation	Nil	Catalysts	(Hosseinzadeh et al. 2017)
Copper (II) acetate	*Lantana camara* flower extract	400 °C	15–40	Spherical	Nil	Nil	Nil	Catalysts	(Chowdhury et al. 2020)
Cu $(CO_2CH_3)_2 \cdot H_2O$	*Azadirachta indica* leaf extract	400 °C	40	Spherical	Nil	Nil	Nil	Nutritive agent	(Anwaar et al. 2016)
Copper nitrate trihydrate	*Black tea* extract	500, 600, 700 and 800 °C	22–39	Spherical	Nil	Nil	Nil	Nil	(Fardood and Ramazani, 2018)
Copper acetate	*Magnolia champaca* floral extract	60 °C	20–40	Spherical	Nil	Nil	Zebrafish embryonic: 90% and 60% viability rate for 350 mg/l and 750 mg/l	Nil	(Santhoshkumar and Shanmugam, 2020)
Cupric nitrate trihydrate	*Caesalpinia bonducella* seedextract	450 °C	Nil	Rice	ZOI for *S. aureus*: 25 mm and *Aeromonas*: 34 mm	ROS generation and particles interaction	Nil	Electrochemical and biological	(Sukumar et al. 2020)

Table 1 (continued)

Precursor	Reducing/capping agent	Calcination temperature °C	Size of NPs (nm)	Shape of NPs	Antimicrobial activity	Killing mechanism	Toxicity	Application	References
Copper sulfate pentahydrate	*Melia azedarach* leaf extract	80 °C	14–20	Nil	ZOI for *E. coli*: 16 mm, *P. mirabilis*: 4 mm, *Salmonella*: 11 mm and *C. tetani*: 7 mm	Nil	Nil	Nil	(Khan and Mateen, 2018)
Copper sulfate pentahydrate	*Morus nigra* leaf extract	80 °C	14–20	Nil	ZOI for *E. coli*: 12 mm, *P. mirabilis*: 13 mm, *Salmonella*: 12 mm and *C. tetani*: 6 mm	Nil	Nil	Nil	(Khan and Mateen, 2018)
Copper sulfate	*Cymbopogon citratus* (CLE) leaf extract	80 °C	11.4–14.5	Spherical, hexagonal and oval	Survival rate of *S. aureus*-1 (MRSA-1): 51.4% at 1500 µg/mL, *S. aureus*-2 (MSSA-2): 32.41% at 1500 µg/mL and *E. coli*-336: 45.27% at 1000 µg/mL	Copper ions	Nil	Biomedical	(Cherian et al. 2020)

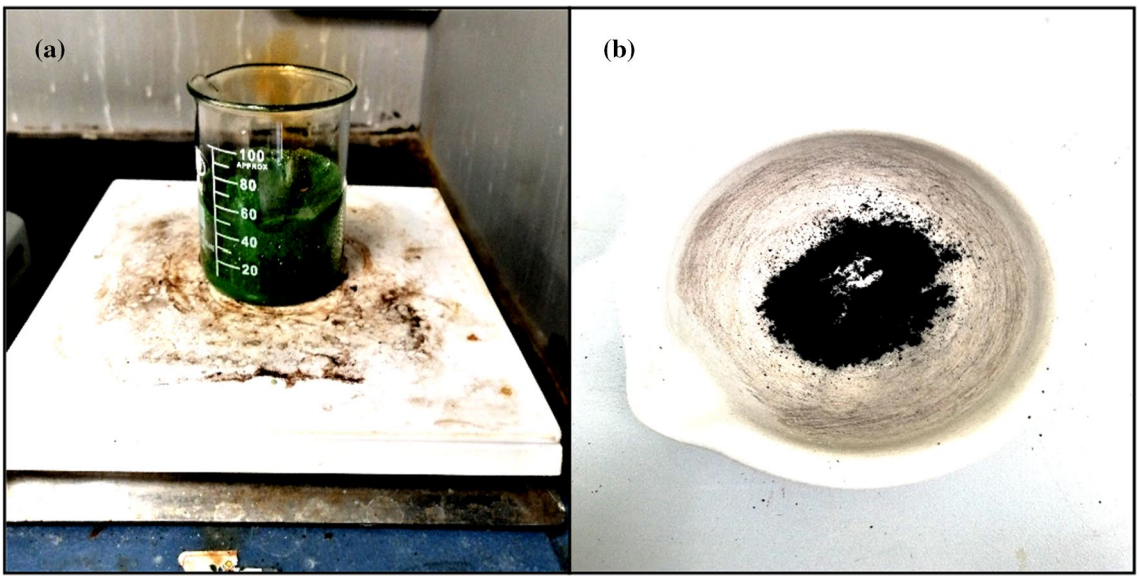

Fig. 1 Green synthesis of CuO nanoparticles; **a** Green paste before annealing and **b** final annealed black CuO powder

USA). Fibroblast was maintained in Roswell Park Memorial Institute (RPMI) 1640 media (Gibco, Life technologies), and the media were supplemented with other nutrients. The alamarBlue™ cell viability reagent DAL1025 (Invitrogen, UK) was used for cell viability assay. 2,2-Diphenyl-1-picrylhydrazyl was purchased from Sigma-Aldrich for DPHH radical scavenging assay. The non-MDR and MDR pathogens of *S. aureus* 29213, *E. coli* 25922, *K. pneumoniae* 700603 and MRSA 38591 were obtained from American Type Culture Collection (ATCC).

Preparation of green-synthesized CuO nanoparticles

Copper (II) nitrate trihydrate was used as main precursor for green synthesis of CuO nanoparticles using giant milkweed plant. The fresh leaves of giant milkweed plant were collected from Perai Pulau Pinang, Malaysia. The species was authenticated by the expert of Unit Herbarium, Pusat Pengajian Sains Kajihayat USM Pulau Pinang (Herbarium No.: 11843). Green CuO nanoparticles were synthesized according to the following procedures (Sharma et al. 2015; Govindasamy et al. 2021a). Copper (II) nitrate trihydrate was dissolved in filtered giant milkweed leaves extracts at boiling temperature of 60–80 °C. The CuO was formed as green paste after the chemical reaction between leaves extracts and copper (II) nitrate trihydrate. The green paste (Fig. 1a) calcined at 400 and 500 °C was called as CuO-400C and CuO-500C, respectively. The final annealed powder gives the appearance of black and very stable monoclinic phase of CuO (Fig. 1b) (Zayyoun et al. 2016). It is proved that green synthesis at calcination temperature between 400 and 500 °C only produces chemically stable CuO without presence of orange Cu_2O powder (Zayyoun et al. 2016).

Characterization of green-synthesized CuO nanoparticles

X-ray diffraction (XRD) patterns of CuO and powdered giant milkweed leaves were recorded with X-ray diffractometer (Bruker D8), and average crystallite sizes of CuO were calculated using Debye–Scherrer equation [1]:

$$d = \frac{K\lambda}{\beta \cos \theta\prime} \quad (1)$$

where λ is the X-ray wavelength of Cu Kα radiation (0.1541 nm), K = 0.9 is the shape factor, β is the FWHM of the respective diffraction peak, and θ is the Bragg diffraction angle. Scanning electron microscopy (SEM Fei Quanta FEG 650) and transmission electron microscopy (TEM FEI TECHNAI F20 G2) were used for the morphology and microstructure observation of the green CuO, respectively. Semi-quantitative analysis of nanoparticles was carried out by energy-dispersive X-ray spectroscopy (EDAX) which is equipped with SEM machine. The primary detection of CuO and natural compound of leaves extract such as carbonyl and phenol group were investigated via UV–Vis spectrophotometer (Varian) in the range of 200–700 nm. The CuO was prepared in a suspension form, by dispersing the powder in autoclaved deionized water for UV–Vis analysis. The functional groups involved in green synthesis and stabilization of CuO were examined using FTIR spectroscopy (Perkin Elmer). The FTIR

spectra of the green samples were recorded in the range of 4000–400 cm^{-1} by the KBr pellet method.

Minimum inhibitory concentration/minimum bactericidal concentration

The MIC/MBC of CuO was determined by the broth dilution technique using 96-well plate as previous protocol (Govindasamy et al. 2021b). The absorbance reading for CuO was determined at appropriate wavelengths before and after 24-h incubation.

Time-kill assay

The bactericidal performance of 20 mg/mL of green CuO-500C sample against time was evaluated toward *S. aureus*, *E. coli* and MRSA according to the following time-kill assay method (Govindasamy et al. 2021b).

Kirby-Bauer disc diffusion assay

Bactericidal activity of green CuO and commercial CuO was evaluated against non-MDR and MDR pathogens using disk-diffusion susceptibility test (El-Kased et al. 2017). Subsequently, 2.5 mg/mL and 10 mg/mL sample's solution was prepared for bactericidal studies.

Cytocompatibility assay ISO 10993–5 (2009)

The fibroblast cells lines model, L929, was cultured in RPMI 1640 media supplemented with 10% (v/v) fetal bovine serum (FBS), 12.5 g/mL HEPES, 1% (v/v) L-glutamine, sodium bicarbonate and 1% (v/v) PenStrep (Gibco, USA). Cells were maintained in T25 flasks and incubated at 37 °C in 5% CO_2 humidified atmosphere and sub-cultured at 80–90% confluency prior experiments. 10% (v/v) of dimethyl sulfoxide (DMSO) was introduced as a negative control (strong cytotoxic material). Blank control (fibroblast cells lines model in culture medium without CuO) was set as 100% viability in the experiment.

Fibroblast cells lines model was used to measure the cytocompatibility of green CuO by calculating cell viability using the alamarBlue™ cell viability reagent DAL1025 (Invitrogen, UK) according to ISO 10993–5 (2009). The cytocompatibility assay was performed following the protocol recommendation in previous study (Harun et al. 2021). Briefly, fibroblast cells lines model was seeded at a density of 1×10^4 cells/well (100 µl/well) in 96-well plate and grown for 24 h in CO_2 incubator at 37 °C. Green CuO was sterilized via autoclave machine at 121 °C prior to use. Then, different-concentrated green CuO (0, 2.5, 5, 10 and 20 mg/mL) was prepared in the culture media and suspension of green CuO nanoparticles was produced. Samples were kept for overnight for facilitating solubility and diffusion of bactericidal ions into media. After that, the suspension of green CuO nanoparticles added into the cells in serial dilution method and incubated for 24 h. The cytocompatibility test was performed in triplicate. After 24 h of incubation period, cell viability was determined using the (1:10) alamarBlue reagent. The cells were incubated for 20 h before measuring the absorbance of viability. The alamarBlue reagent stained treated fibroblast cells lines model (blank alamarBlue reagent media without cells and green CuO) was detected absorbance at wavelength 570 nm and 600 nm using a microplate reader (Bio-Tek Instruments, USA) (Harun et al. 2021). The absorbance reading from sedimentation of green CuO at bottom surface of well plate can be avoided by transferring color changed and increased fluorescence alamarBlue reagent media into new 96-well plate before reading the actual absorbance. The morphology of the cells was captured through an Olympus CKX41 optical light microscope, and images are taken with magnification of 20 X.

DPHH radical scavenging assay

The antioxidant activity of the giant milkweed leaf extract aqueous solution samples was determined by the DPPH (2,2-diphenyl-1-picrylhydrazyl, Sigma-Aldrich) assay as previously reported by Sachett et al. 2021. Absolute ethanol was labeled as negative control. DPHH control without treatment was introduced as well. Total five replicate sample solutions for each treatment were prepared using aluminum foil wrapped 1.5-mL microtubes and incubated at 25 °C for 24 h in the dark environment. Then, all the treated solutions were transferred into 96-well microplate and the absorbance (Abs) of the samples was read at 517 nm in a microplate spectrophotometer. The percentage of DPHH scavenging effect was measured using the Equation [2]:

$$\text{DPHH}\ (\%) = \frac{\text{Abs control DPHH - (Abs sample - Abs negative control)}}{\text{Abs control DPHH}} \times 100 \quad (2)$$

Statistical analysis

Statistical significance was determined by two-way ANOVA implemented in the GraphPad Prism. Results were considered statistically significant if P value is less than 0.05 with respect to control. Data are presented as

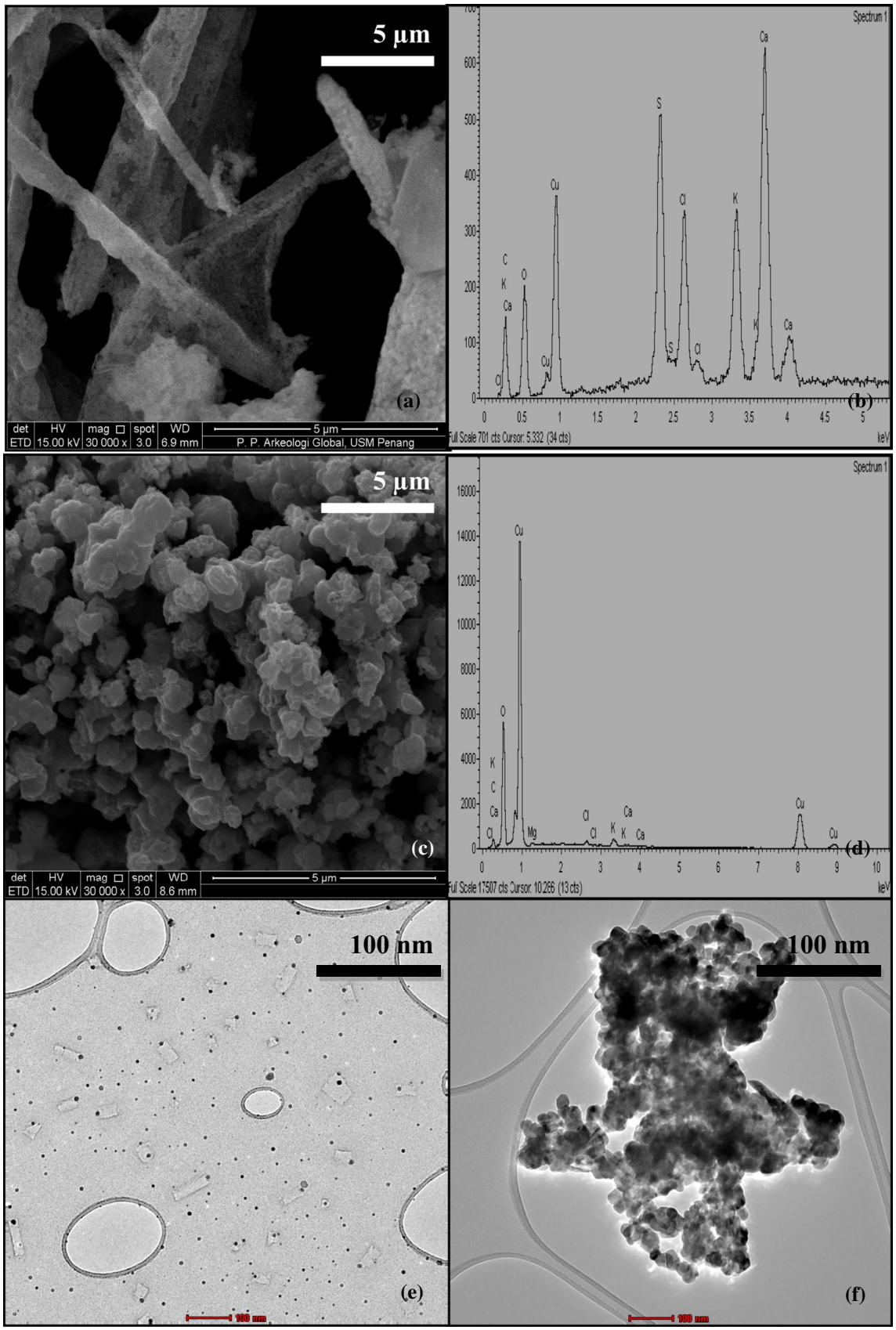
5 µm
(a)
det HV mag spot WD
ETD 15.00 kV 30 000 x 3.0 6.9 mm
5 µm
P. P. Arkeologi Global, USM Penang
Spectrum 1
Ca
S
Cu
Cl
K
C
O
(b)
keV
5 µm
(c)
det HV mag spot WD
ETD 15.00 kV 30 000 x 3.0 8.6 mm
5 µm
Spectrum 1
Cu
O
K
C
Ca
Cl
Mg
(d)
keV
100 nm
(e)
100 nm
(f)

◂**Fig. 2** SEM and TEM analysis on green-synthesized CuO; **a** SEM micrograph of CuO-400C (5 µm), **b** EDAX spectrum of CuO-400C, **c** SEM micrograph of CuO-500C (5 µm), **d** EDAX spectrum of CuO-500C, **e** TEM micrograph of CuO-400C (100 nm) and **f** TEM micrograph of CuO-500C (100 nm)

mean values of three independent replicates (n = 3) and standard deviation (± SD).

Results and discussion

Characterization of the green-synthesized CuO nanoparticles

The morphology of the green CuO was studied using scanning electron microscopy (SEM) and transmission electron microscopy (TEM) and is shown in Fig. 2. The TEM average particle size of CuO nanoparticles was measured by ImageJ software analysis. The SEM and TEM images (Figs. 2a, c, e and f) show that the CuO-400C sample is a mixture of rod- and quasi-spherical-shaped nanoparticles and the CuO-500C sample is oval in shape with agglomerated nanosized morphology.

In this step, energy-dispersive spectroscopy (EDAX) analysis was used to evaluate the chemical composition and purity of the prepared samples. The EDAX analysis of the bioderived CuO confirms the presence of Cu and O, which are about 17.52 and 17.92 wt.%, respectively, in CuO-400C and 67.23 and 25.05 wt.%, respectively, in CuO-500C (Figs. 2b and d). The Cu and O atoms in the EDAX profile of CuO exhibit strong signals. High chemical weight composition in Cu ratio for CuO-500C sample was formed during green synthesis, and it might be correlated to the complete crystallization of monoclinic pure CuO at high annealing temperature of 500 °C (Luna et al. 2015). Formation of some additional peaks was natural bioderived elements from giant milkweed plant. The presence of the weak peaks of C, Ca, S, Cl, K and Mg atoms in the green CuO indicates the participation of the phytochemical compounds in giant milkweed leaf extract during the green synthesis (Bharathi et al. 2020; Fafal et al. 2017; Kannan et al. 2013; Majeed et al. 2021) (Table 2).

The diffraction peaks with Miller indices of CuO-400C and CuO-500C samples are presented in Fig. 3a. CuO-400C and CuO-500C have 12 main diffraction peaks at 32.32°, 35.50°, 38.71°, 45.01°, 48.37°, 53.29°, 58.15°, 61.09°, 65.56°, 67.90°, 72.16° and 75.13°, which correspond to the crystal faces (110), (− 111), (111), (202), (− 202), (020), (202), (− 113), (− 311), (220), (311) and (004), respectively. The green CuO nanoparticles have a monoclinic crystalline structure (ICDD number 01–089-5897) with the following lattice constant: a = 4.686486, b = 3.421156, c = 5.129263, α = 90°, β = 99.413°, γ = 90° along with d-spacing value of 2.52761 Å. Previously Ravele et al. (2022) stated that formation of monoclinic pure phase of CuO only obtained at calcination temperature above 350 °C. But, cubic phase of Cu_2O or other Cu oxide mixture could appear when the nanoparticles produced at low calcination temperature below than 300 °C (Ravele et al. 2022). Basically, in this study, it confirms the green synthesis of pure CuO nanoparticles with monoclinic geometry. The X-ray diffraction peaks at 28.80°, 31.53°, 40.94°, 50.47°, 58.89°, 66.70°, 67.70° and 73.92° observed in the control powdered giant milkweed leaf sample (Fig. 2a) demonstrated that the medicinal plant is rich in bioderived constituents, mainly carbon (C) and calcium (Ca). These natural compounds could further accelerate the bactericidal activity of CuO synergistically (Mydin et al. 2018; Marquis et al. 2015; Dizaj et al. 2015). The crystallite size of CuO was estimated from the XRD pattern using Scherer's equation at the highest FWHM peak (Table 3).

Fourier transform infrared spectroscopy was performed to investigate the participation of phytochemical compounds in stabilizing and reducing green CuO (Fig. 3b). The sharp peak at 3438 cm^{-1} is assigned to O–H stretching polyphenols (flavonoids). In future, high-performance liquid chromatography (HPLC) method is recommended to further identify and quantify the flavonoids and phenolic compounds of giant milkweed leaves extract aqueous solution. This flavonoids compounds may act as a capping and reducing agent, thus providing greatest stability in the formation of green CuO during green synthesis (Hublikar et al. 2021a, b). The peaks between 1633 and 1765 cm^{-1} are assigned to the C = C (carbonyl group) and C = O stretching. The absorption peaks at 1385 cm^{-1} are assigned to the vibration mode of esters. The absorption peaks between 1110 and 1115 cm^{-1} belong to the C–O stretching of bioderived elements of giant milkweed leaf extract (Siddiqi and Husen, 2020; Bhavyasree and Xavier, 2020). The low absorption peak at 540 cm^{-1} is a characteristic peak of the CuO group (Das et al. 2018; Fouda et al. 2020). The intensity of broad absorbance peak of O–H stretching at 3438 cm^{-1} and small peaks of C = C and C = O stretching between 1633 and 1765 cm^{-1} were sharply decreased as calcination temperature increased to 500 °C, thus suggesting condensation of $Cu(OH)_2$ into pure CuO phase with removal of water molecules (Hamid et al. 2021). The reduction of ionic copper into copper nanoparticles was successfully obtained under the effect of carbonyl and hydroxyl compounds in the giant milkweed leaves extract aqueous solution.

The UV–Vis spectrogram of giant milkweed extract and green CuO is shown in Fig. 3c. Giant milkweed extract as the control solution has two prominent absorbance peaks at 206 (carbonyl compounds) and 269 nm (phenolic compounds) in the UV spectrum (Mongkholrattanasit et al. 2011). The solution with CuO has a sharp distinct absorbance peak at

Table 2 SEM-EDAX chemical weight composition (%) results for different calcined CuO

Sample	C	O	Mg	Cl	K	S	Ca	Cu
CuO-400C	16.67	17.92	–	7.44	9.7	8.83	21.92	17.52
CuO-500C	5.28	25.05	0.34	0.59	1.28	–	0.23	67.23

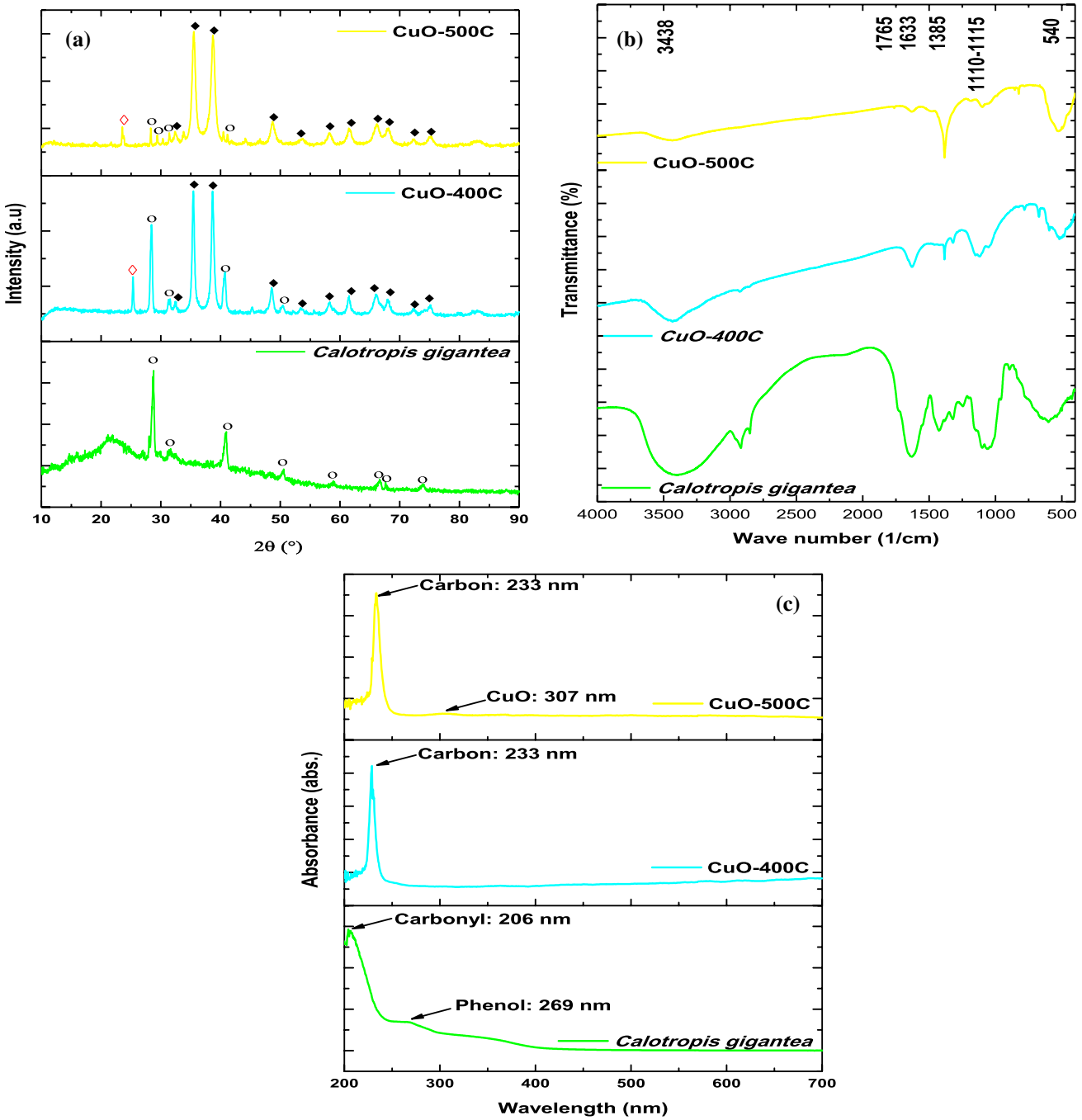

Fig. 3 **a** XRD diffraction peaks of green-synthesized CuO [: *C. gigantea* leaves, CuO, *filled diamond*: additional peaks appeared after green synthesis]; **b** FTIR spectra of green CuO; and **c** UV–Vis absorbance spectra of green CuO

Table 3 CuO nanoparticles size and shape

Sample	Crystallite size (nm)	Average particle size (nm)	Grain shape
CuO-400C	24.1	Rod = Length: 58.46 ± 4.00, width: 24.13 ± 1.439; quasi-spherical: 9.73 ± 0.602	Rod and quasi-spherical
CuO-500C	24.1	Diameter: 25.48 ± 1.433, length: 21.25 ± 1.149	Oval

Table 4 MIC and MBC of green CuO against various skin pathogen associated with open wound infections

Strain	Samples	MIC (mg/mL)	MBC (mg/mL)
S. aureus	CuO-400C	5	20
	CuO-500C	5	20
E. coli	CuO-400C	1.25	20
	CuO-500C	0.625	5
K. pneumoniae	CuO-400C	10	20
	CuO-500C	1.25	5
MRSA	CuO-400C	10	20
	CuO-500C	0.3125	2.5

233 nm, which belongs to natural carbon (Son and Park, 2018). The produced nanoparticles can be identified by the appearance of a small band at around 307 nm in their respective spectra for the CuO-500C (Siddiqi and Husen, 2020). This similar trend was previously identified by Bharathi et al. (2019).

Minimum inhibitory concentration (MIC) and minimum bactericidal concentration (MBC)

Skin-associated pathogens are a global public health threat, and the wound care and management of serious wounds incur huge economic costs. *S. aureus*, *E. coli*, *K. pneumoniae* and MRSA are the prevailing microbial pathogens that occur in patients with open colonized wounds. Gram-positive *S. aureus* is among the most common skin pathogens associated with open wound infections (Dunyach-Remy et al. 2016). So, this study mainly focuses on investigating the bactericidal performance of green CuO-400C and CuO-500C toward Gram-positive (*S. aureus*), Gram-negative (*E. coli*) and other MDR pathogens (*K. pneumoniae* and MRSA).

The preliminary screening MIC and MBC study concentrates on determining bactericidal activity of CuO-400C and CuO-500C against skin pathogens such as *S. aureus*, *E. coli*, *K. pneumoniae* and MRSA. The MIC and MBC results against non-MDR and MDR strains are shown in Table 4 and Fig. 4. It was clearly noticed that a significant decrease in *S. aureus* colony count from 4.3 $\log_{10}$ to 2.72 $\log_{10}$ at concentration of 10 mg/mL for CuO-500C was seen (Figure S1; Supplementary material). But for CuO-400C sample did not show any bactericidal activity at dosage of 10 mg/mL (Figure S1; Supplementary material); thus, it considered less effective in killing toward *S. aureus* at low concentration. However, the MBC of CuO-400C and CuO-500C for *S. aureus* is 20 mg/mL. The results showed that CuO-400C, which was produced at low annealing temperature, is less effective in killing microbes at low dosage compared with CuO-500C because of its reduced specific surface area (SSA) (Damm et al. 2008). In general, CuO nanoparticles exhibited shape-dependent bactericidal activity toward various bacterial strains (Laha et al. 2014; Tavakoli et al. 2019). The strong bactericidal effect of CuO-500C might be attributed to the highest SSA of uniform oval-shaped pure monoclinic CuO produced at high calcination temperature (Lee et al. 2021).

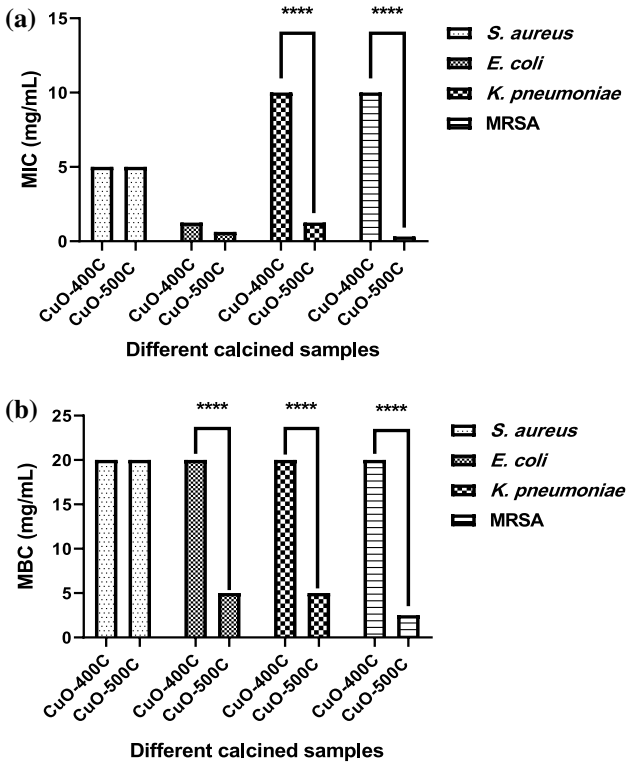

Fig. 4 Evolution of MIC and MBC of green CuO-400C and CuO-500C toward *S. aureus*, *E. coli*, *K. pneumoniae* and MRSA; **a** MIC results and **b** MBC results. Statistical significance was calculated using analysis of two-way ANOVA (GraphPad Prism). ****$P < 0.0001$

In addition, the bactericidal performance of CuO against non-MDR Gram-negative and MDR pathogens was further investigated. Based on MIC result shows that the CuO-500C was most potent bactericidal agent in tackling *E. coli*, *K. pneumoniae* and MRSA at lowest concentration level ranging from 0.3125 to 5 mg/mL, while CuO-400C bactericidal activity ability was depending on the higher concentration level (1.25–10 mg/mL). This study recommends that the killing mechanisms of CuO toward different species of pathogens should be further investigated. We concluded that CuO-500C, which has uniform oval shape, is a more potential bactericidal agent than CuO-400C. The rate of the bacterial killing activity was further improved for green-synthesized CuO-500C sample, and it might be due to closer interaction established between the small nanosized and high surface area to volume ratio of the bioderived oval-shaped CuO and bacterial outer cell membrane (Mahamuni et al. 2019; Dulta et al. 2022). The strong bactericidal effectiveness of green CuO-500C is most likely due to the pronounced copper ion release (Cu^{2+}) (Govindasamy et al. 2021c) and oxidative stress caused by ROS (Fouda et al. 2020). Meanwhile, mixture of large-sized rod-shaped CuO-400C sample with length of 58.46 ± 4.00 nm expected to have smaller surface-to-volume ratio, resulting in fewer Cu^{2+} ions release than uniform oval-shaped CuO-500C sample with diameter of 25.48 ± 1.433 nm (Table 3) (Naqvi et al. 2019). Bacterial metabolism process might be disrupted when Cu^{2+} ions effectively interact and bind the DNA molecules, leading to helical structure disorder (Dulta et al. 2022).

Time-kill assay

The time-dependent bactericidal activity of the optimized green CuO-500C was determined against non-MDR and MDR skin pathogens. In this investigation, we have only studied the time-kill bactericidal performance of CuO-500C sample against selected skin pathogens based on the results obtained from the preliminary study of MIC and MBC (Table 4) and cytocompatibility study (Fig. 7). The non-toxic behavior and lowest MIC value of CuO-500C sample create a great extent for utilization of this green-synthesized nanoparticles as strong bactericidal agent in future biomedical field. The outcomes of the experiment are shown in Fig. 5 and Fig. 6. A ≤ 2.5 $\log_{10}$ reduction in *S. aureus* colonies proportional with time was observed in those treated with the green CuO-500C. A reduction in *S. aureus* viable count from 4.3 $\log_{10}$ to 2.3 $\log_{10}$ after 6 h (Fig. 5c) and complete killing at 12 h (Fig. 5d) was recorded. The average log reduction of the *E. coli* colonies at 3.3 $\log_{10}$ cfu/mL was seen after 6 h of incubation and bactericidal effect was attained at 12 h (Figs. 5h and i). However, MRSA growth inhibition was more apparent at 12 h of incubation, with complete inactivation at 24 h (Figs. 5n and o). The killing activity of CuO-500C was strain-dependent where it required prolonged period (up to 24 h) to attain bactericidal effect against pathogenic MDR MRSA strain (Kannan et al. 2021). The untreated *S. aureus*, *E. coli* and MRSA skin pathogen revealed no decrease in colony counts after 24 h of incubation.

The growth rate of the skin pathogens was further assessed via optical density measurement through microplate reader (Bio-Tek Instruments, USA) at 570 nm after 24-h incubation with CuO-500C, and the result is presented in Fig. 6. As it is seen from Fig. 6, the cloudy bacterial media (control strain) turned into transparent and clear blue color solution with presence of CuO, indicating an absence of bacterial colonies and decomposition of CuO. Moreover, the absorbance reading had been dropped significantly for CuO-500C treated samples. Overall the results of the time-kill analysis showed that a remarkable reduction in non-MDR and MDR colonies was achieved between 12 and 24 h of exposure. The bactericidal action of the green CuO might be from the release of free metal oxide ions and the generation of ROS ($\bullet O^{2-}$, $\bullet OH^{-}$, Cu^{2+} and Ca^{2+}) which lead to severe rupture of cell membranes of bacteria (Jadhav et al. 2017; Yang et al. 2018b, a). Further investigation on metal ion release (Cu^{2+}) and generation of ROS is recommended.

Kirby–Bauer disc diffusion test

The bactericidal activities of green CuO and commercial CuO at two different concentrations (2.5 and 10 mg/mL), as well as giant milkweed leaf extract, were examined on *S. aureus*, *E. coli*, *K. pneumoniae* and MRSA. The diameter ZOI reveals that CuO-500C was effective toward skin pathogen as the concentration increased from 2.5 mg/mL to 10 mg/mL. The MIC and MBC results agree with the finding that the bactericidal effectiveness of CuO is concentration-dependent (Table 5 and Figure S2; Supplementary material). The results of the Kirby–Bauer disc diffusion showed that the bactericidal activity of 10 mg/mL green CuO-500C was greater than those of other samples. CuO-500C at concentration 10 mg/mL against skin pathogens produced respective inhibition zones between 6.50 ± 0.00 and 7.33 ± 0.33 mm. Comparatively, commercial CuO had smaller zone of inhibition which ranges from 6 to 6.25 mm at 10 mg/mL. The increased bactericidal activity might be attributed to the increase in free metal oxide ions and ROS along with bioderived elements (C and Ca) at higher dosage.

Cytocompatibility study

Cytocompatibility of green CuO has been studied on the fibroblast cells lines model (Fig. 7 and Figure S3; Supplementary material). The fibroblast cells lines were able to survive and proliferate healthily above 90% after 24-h

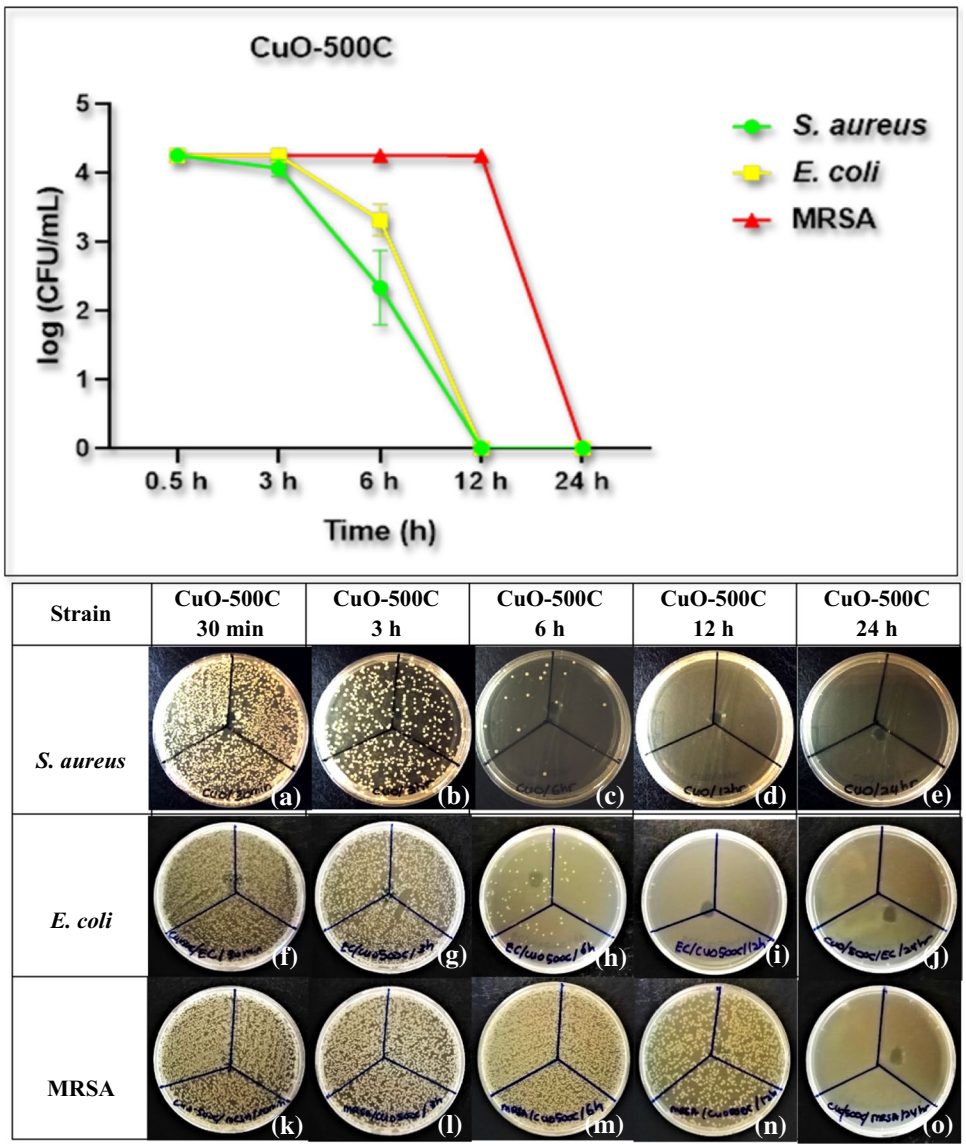

Fig. 5 Time-kill assay showing bactericidal activity exhibited by 20 mg/mL of CuO-500C against different skin pathogens for 0.5-h (30 min), 3-h, 6-h, 12-h and 24-h treatment periods; **a** CuO-500C at 0.5 h (30 min) against *S. aureus*, **b** CuO-500C at 3 h against *S. aureus*, **c** CuO-500C at 6 h against *S. aureus*, **d** CuO-500C at 12 h against *S. aureus*, **e** CuO-500C at 24 h against *S. aureus*, **f** CuO-500C at 0.5 h (30 min) against *E. coli*, **g** CuO-500C at 3 h against *E. coli*, **h** CuO-500C at 6 h against *E. coli*, (**i**) CuO-500C at 12 h against *E. coli*, **j** CuO-500C at 24 h against *E. coli,* **k** CuO-500C at 0.5 h (30 min) against MRSA, **l** CuO-500C at 3 h against MRSA, **m** CuO-500C at 6 h against MRSA, **n** CuO-500C at 12 h against MRSA and **o** CuO-500C at 24 h against MRSA

incubation with addition of 2.5–10 mg/mL of CuO-500C and 2.5–5 mg/mL of CuO-400C. Most of the cell lines were highly deteriorated and appeared in dull, shrink, rounded shape with reduction in cells density when high concentrated of CuO-500C (20 mg/mL) and CuO-400C (10–20 mg/mL) was introduced. Conversely, healthy live cells appeared in extended proliferation with elongated filopodia as referred to control cell line without an addition of CuO (blank control). Comparatively, 10% (v/v) DMSO had a strong cytotoxic effect on fibroblast cells lines. The sedimentation of agglomerated CuO appeared to be black, as indicated by yellow circle in the image.

Our cell viability experiment demonstrated that the green-synthesized CuO-500C and CuO-400C were shown concentration-dependent cytocompatibility effect toward fibroblast cells lines where at high doses the cell line was severely affected and induced abnormal morphologies. It might be attributed to the higher release of free radicals at high dosage level (Ayoubi et al. 2017). It is believed that overproduced hydroxyl radicals in short duration of time have reactive and hazardous free radicals which causes disturbance to wound healing-related cells and fibroblast (Fu et al. 2014). However, the natural carbon and calcium-wrapped CuO-500C at concentration of 2.5–10 mg/mL might prolong the release time of free radicals in steady manner for long-term bactericidal application and create stable environment that might provide cytocompatibility advantage (Yang et al. 2018b, a). Successful control on steady and slow release of free radicals such as $\bullet O^{2-}$ and $\bullet OH^{-}$ from this green-synthesized nanoparticle might present with cytocompatibility properties toward human cells and can accelerate wound healing properties (Sung et al. 2020).

Generally, shape and size of nanoparticles play an important role in effecting cell viability (Yin et al. 2012;

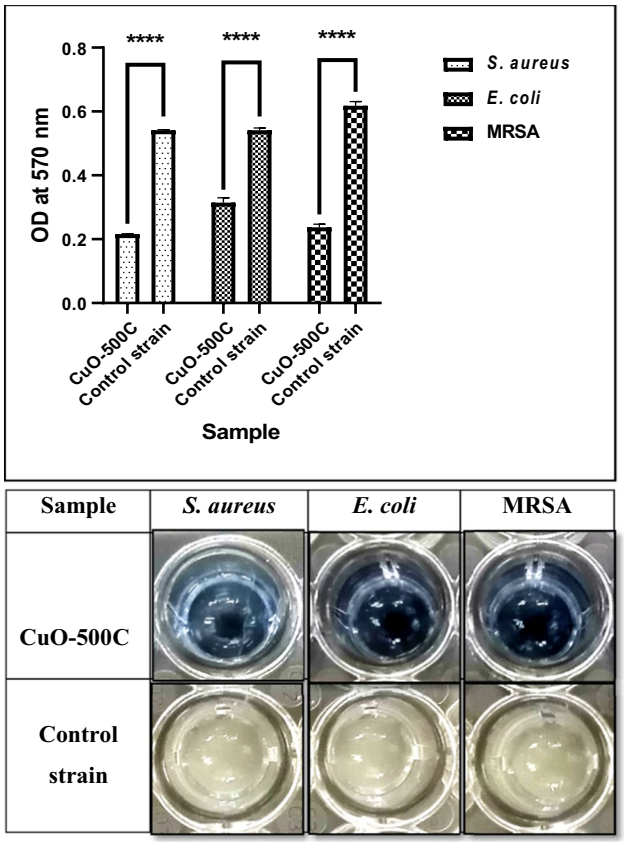

Fig. 6 Optical density (OD) measurement at 570 nm measured after 24-h incubation with CuO-500C. These data represent mean (±SD) of three replicates. Statistical significance was calculated using analysis of two-way ANOVA (GraphPad Prism). ****$P<0.0001$

Table 5 Measurement of the diameter zone of inhibition of CuO against skin pathogen. "NA" be a sign of no bactericidal activity observed for this sample

Strain	Sample	ZOI (mm) at 2.5 mg/mL	ZOI (mm) at 10 mg/mL
S. aureus	CuO-400C	6 ± 0.00	7 ± 0.00
	CuO-500C	6 ± 0.00	7.33 ± 0.33
	Commercial CuO	6 ± 0.00	6.17 ± 0.17
	Giant milkweed	6.33 ± 0.17	
	Negative control	NA	
	Positive control	10 ± 0.00	
E. coli	CuO-400C	6 ± 0.00	6 ± 0.00
	CuO-500C	6 ± 0.00	6.50 ± 0.50
	Commercial CuO	6 ± 0.00	6 ± 0.00
	Giant milkweed	6.00 ± 0.00	
	Negative control	NA	
	Positive control	10 ± 0.00	
K. pneumoniae	CuO-400C	6 ± 0.00	6 ± 0.00
	CuO-500C	6 ± 0.00	6.50 ± 0.00
	Commercial CuO	6 ± 0.00	6.25 ± 0.00
	Giant milkweed	6.15 ± 0.00	
	Negative control	NA	
	Positive control	9 ± 0.00	
MRSA	CuO-400C	6 ± 0.00	6 ± 0.00
	CuO-500C	6.17 ± 0.14	6.67 ± 0.29
	Commercial CuO	6 ± 0.00	6.25 ± 0.00
	Giant milkweed	6.15 ± 0.00	
	Negative control	NA	
	Positive control	8 ± 0.00	

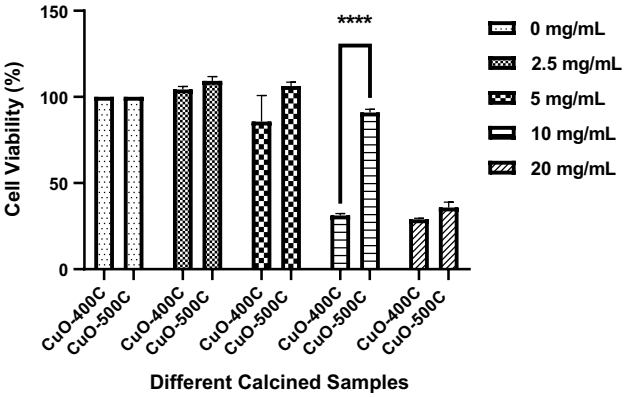

Fig. 7 Effect of different concentrated green CuO-400C and CuO-500C on cytocompatibility of fibroblast cells lines ($n=3$). Statistical significance was calculated using analysis of two-way ANOVA (GraphPad Prism). ****$P<0.0001$

Sirelkhatim et al. 2016). The findings noticeably revealed the difference of size and shape between CuO-500C and CuO-400C in responding to cell cytocompatibility. Smaller size (< 10 nm) and dominant quasi-spherical-like structures CuO-400C displayed strong cytotoxic effects toward fibroblast cells lines at concentration of 10 mg/mL (Yin et al. 2012; Sirelkhatim et al. 2016), while uniform oval-shaped CuO-500C (~ 20 nm) offer better cell proliferation and maintain live cells up to 90% in wound healing. We believed that smaller size dominant quasi-spherical-like structures CuO-400C might further accelerate uncontrollable amounts of ROS release at elevated level and promote inhibition of cell growth (Yin et al. 2012; Sirelkhatim et al. 2016). However, high-concentrated green CuO can be safely introduced to the cells by embedding them into biopolymer like chitosan for future biomedical application (Gopal et al. 2014). Collectively, these outcomes exhibited that CuO-500C would be suitable candidates for wound healing application at low dosage level (2.5–10 mg/mL). Finally, further investigation on the long-term (48–72 h) cytocompatibility effect of CuO-500C on fibroblast cells lines is recommended.

Table 6 Storage-dependent DPHH scavenging (%) for giant milkweed leaf extract solutions

Sample	DPHH scavenging (%)
Giant milkweed—1 year	52.85
Giant milkweed—2 year	35.05

DPHH assay

The storage-dependent antioxidant assay for giant milkweed leaf extract solutions was evaluated according to the in vitro protocol illustrated by Sachett et al. 2021. As shown in Table 6, giant milkweed leaf extract aqueous solution which stored at –4 °C for approximately 1 year and 2 years, presented the free radical scavenging activity of 52.85 and 35.05%, respectively. This observation revealed that prolongation of storage time could decrease the bioactive elements from giant milkweed leaf extract aqueous solution (Xu et al. 2018). Hence, the storage condition plays a vital role in determining inhibition of the DPPH radical.

Conclusions

This study revealed the potential of bioderived natural constituents decorated on plant-mediated copper oxide (CuO-500C) nanoparticles from giant milkweed as strong bactericidal agent against non-MDR and MDR wound-associated pathogens. This bactericidal agent worked effectively in a concentration-dependent manner and demonstrated strong killing effect against *S. aureus*, *E. coli*, *K. pneumoniae* and MRSA. The outcome of the cytocompatibility study on fibroblast cells lines model proved that the low-concentrated CuO-500C (2.5 – 10 mg/mL) had cell viability of approximately above 90% at 24-h treatment. A further understanding on the killing mechanism of CuO-500C toward skin pathogens, especially on metal oxide ion and ROS release profile, is needed. In addition, the cell viability study for longer period (48 – 72 h) should be carried out in future to understand the long-term cytocompatibility effect of green CuO-500C toward fibroblast cells lines model.

Supplementary Information The online version contains supplementary material available at https://doi.org/10.1007/s11696-022-02513-5.

Acknowledgements The authors would like to thank Universiti Sains Malaysia for sponsoring this work under Research University Grant (RUI) EKSESAIS TAHUN 2019 (1001/CIPPT/8012338). The support of all the technical staff of Advanced Medical and Dental Institute and School of Materials and Mineral Resources Engineering, Universiti Sains Malaysia, Pulau Pinang, Malaysia, in the characterization of the sample is also acknowledged.

Authors' contributions GAG contributes in the writing of this manuscript and carried out all experimental works. NHH, WNFWEE and SS assist in the procedures. RBSMNM is the principal investigator contributing in the concept, idea, experimental design, writing process and gave final approval of this paper for publication. All authors have given approval to the final version of the manuscript.

Funding This research was funded by the Research University Grant (RUI) EKSESAIS TAHUN 2019 (1001/CIPPT/8012338) from Universiti Sains Malaysia.

Availability of data and materials The datasets generated and/or analyzed during the current study are not publicly available due to the patent application for methods of making and using of copper oxide formed by green synthesis but are available from the corresponding author on reasonable request.

Declarations

Conflict of interest The authors declare no conflict of interest.

Consent for publication Not applicable.

References

Aminuzzaman M, Kei LM, Liang WH (2017) Green synthesis of copper oxide (CuO) nanoparticles using banana peel extract and their photocatalytic activities. AIP Conf Proc 1828:020016

Altikatoglu M, Attar A, Erci F, Cristache CM, Isildak I (2017) Green synthesis of copper oxide nanoparticles using *Ocimum Basilicum* extract and their antibacterial activity. Fresenius Environ Bull 26(12):7832–7837

Apriandanu DOB, Yulizar Y (2019) *Tinospora crispa* leaves extract for the simple preparation method of CuO nanoparticles and its characterization. Nano Struct Nano Objects 20:100401

Asemani M, Anarjan N (2019) Green synthesis of copper oxide nanoparticles using *Juglans regia* leaf extract and assessment of their physico-chemical and biological properties. Green Process Synth 8:557–567

Acharyulu NPS, Dubey RS, Swaminadham V, Kollu P, Kalyani RL, Pammi SVN (2014) Green synthesis of CuO nanoparticles using *Phyllanthus Amarus* leaf extract and their antibacterial activity against multidrug resistance bacteria. Int J Eng Res Technol 3(4):639

Anwaar S, Maqbool Q, Jabeen N, Nazar M, Abbas F, Nawaz B, Hussain T, Hussain SZ (2016) The effect of green synthesized CuO nanoparticles on callogenesis and regeneration of *Oryza sativa* L. Front Plant Sci 7(1330)

Akintelu SA, Folorunso AS, Folorunso FA, Oyebamiji AK (2020) Green synthesis of copper oxide nanoparticles for biomedical application and environmental remediation. Heliyon 6(7):e04508

Azam A, Ahmed AS, Oves M, Khan MS, Adnan Memic A (2012) Size-dependent antimicrobial properties of CuO nanoparticles against Gram-positive and -negative bacterial strains. Int J Nanomed 7:3527–3535

Azizi S, Mohamad R, Bahadoran A, Bayat S, Rahim RA, Ariff A, Saad WZ (2016) Effect of annealing temperature on antimicrobial and structural properties of Bio-synthesized Zinc Oxide Nanoparticles Using Flower Extract of *Anchusa italic*. J Photochem Photobiol B Biol 161:441–449

Ayoubi M, Naserzadeh P, Hashemi MT, Reza Rostami M, Tamjid E, Tavakoli MM, Simchi A (2017) Biochemical mechanisms of dose-dependent cytotoxicity and ROS-mediated apoptosis induced by lead sulfide/graphene oxide quantum dots for potential bioimaging applications. Sci Rep 7(1):12896

Berra D, Laouini SE, Benhaoua B, Ouahrani MR, Berrani D, Rahal A (2018) Green synthesis of copper oxide nanoparticles by *Pheonix Dactylifera L* leaves extract. Dig J Nanomater Biostruct 13(4):1231–1238

Bharathi D, Ranjithkumar R, Chandarshekar B, Bhuvaneshwari V (2019) Bio-inspired synthesis of chitosan/copper oxide nanocomposite using rutin and their anti-proliferative activity in human lung cancer cells. Int J Biol Macromol 141:476–483

Bharathi, D., Preethi, S., Abarna, K., Nithyasri, M., Kishore, P., and Deepika, K. (2020) Bio-inspired synthesis of flower shaped iron oxide nanoparticles (FeONPs) using phytochemicals of *Solanum lycopersicum* leaf extract for biomedical applications. Biocatal Agric Biotechnol 101698

Bhavyasree PG, Xavier TS (2020) Green synthesis of Copper Oxide/Carbon nanocomposites using the leaf extract of AdhatodavasicaNees, their characterization and antimicrobial activity. Heliyon 6(2):e03323

Bogoslovskaya OA, Olkhovskaya IP, Ovsyannikova MN et al (2022) Modern wound-healing gels with antibacterial properties based on copper nanoparticles. Nanobiotechnol Rep 17:211–218

Chowdhury R, Khan A, Rashid MH (2020) Green synthesis of CuO nanoparticles using *Lantana camara* flower extract and their potential catalytic activity towards the aza-Michael reaction†. RSC Adv 10:14374

Cherian T, Ali K, Saquib Q, Faisal M, Wahab R, Musarrat J (2020) *Cymbopogon Citratus* functionalized green synthesis of CuO-nanoparticles: novel prospects as antibacterial and antibiofilm Agents. Biomolecules 10(169)

Djavid GE, Tabaie SM, Tajali SB, Totounchi M, Farhoud A, Fateh M, Ghafghazi M, Koosha M, Taghizadeh S (2020) Application of a collagen matrix dressing on a neuropathic diabetic foot ulcer: a randomised control trial. J Wound Care WUWHS Suppl 29(3)

Dizaj SM, Mennati A, Jafari S, Khezri K, Adibkia K (2015) Antimicrobial Activity of Carbon-Based Nanoparticles. Adv Pharm Bull 5(1):19–23

Das P, Ghosh S, Ghosh R, Dam S, Baskey (Sen) M (2018) Madhuca longifolia plant mediated green synthesis of cupric oxide nanoparticles: a promising environmentally sustainable material for wastewater treatment and efficient antibacterial agent. J Photochem Photobiol B Biol 189:66–73

Dunyach-Remy C, Essebe CN, Sotto A, Lavigne J (2016) *Staphylococcus aureus* toxins and diabetic foot ulcers: role in pathogenesis and interest in diagnosis. Toxins 8(209)

Damm C, Munstedt H, Rosch A (2008) The Antimicrobial efficacy of polyamide 6/silver-nano- and microcomposites. Mater Chem Phys 108:61

Dulta K, Koşarsoy Ağçeli G, Chauhan P et al (2022) Multifunctional CuO nanoparticles with enhanced photocatalytic dye degradation and antibacterial activity. Sustain Environ Res 32:2

El Desouky FG, Saadeldin MM, Mahdy MA, El Wahab SMA, El Zawawi IK (2020) Impact of calcination temperature on the structure, optical and photoluminescence properties of Nanocrystalline Cerium oxide thin films. Mater Sci Semicond Process 111:104991

El-Kased RF, Amer RI, Attia D, Elmazar MM (2017) Honey-based hydrogel: In vitro and comparative In vivo evaluation for burn wound healing. Sci Rep 7:9692

Fafal T, Tastan P, Tuzun BS, Ozyazici M, Kivcak B (2017) Synthesis, characterization and studies on antioxidant activity of silver nanoparticles using *Asphodelus aestivus* Brot. aerial part extract. S Afr J Bot 112:346–353

Fardood ST, Ramazani A (2018) Black Tea Extract Mediated Green Synthesis of Copper Oxide Nanoparticles. J Appl Chem Res 12(2):8–15

Frykberg RG, Banks J (2015) Challenges in the Treatment of Chronic Wounds. Adv Wound Care 4(9):560

Fouda A, Salema SS, Wassel AR, Hamza MF, Shaheen TI (2020) Optimization of green biosynthesized visible light active CuO/ZnO nano-photocatalysts for the degradation of organic methylene blue dye. Heliyon 6:e04896

Fu PP, Xia Q, Hwang H, Ray PC, Yu H (2014) Mechanisms of nanotoxicity: Generation of reactive oxygen species. J Food Drug Anal 22:64–75

Fuku X, Modibedi M, Mathe M (2020) Green synthesis of Cu/Cu_2O/CuO nanostructures and the analysis of their electrochemical properties. SN Appl Sci 2:902

Govindasamy, G. A, Mydin, R. B. S. M. N., Sreekantan, S. and Harun, N. H. (2021a) Effect of calcination temperature on physicochemical and antimicrobial properties of green synthesised ZnO/C/Ca nanocomposites using *Calotropis gigantea* leaves. Adv Nat Sci Nanosci Nanotechnol 12(1):015013

Govindasamy GA, Mydin RBSMN, Sreekantan S et al (2021b) Compositions and antimicrobial properties of binary ZnO–CuO nanocomposites encapsulated calcium and carbon from *Calotropis gigantea* targeted for skin pathogens. Sci Rep 11:99

Govindasamy GA, Mydin RBSMN, Sreekantan S et al (2021c) Bactericidal potential of dual-ionic honeycomb-like ZnO-CuO nanocomposites from *Calotropis gigantea* against prominent pathogen associated with skin and surgical wound infections: *Staphylococcus aureus*. Mater Sci Energy Technol 4:383–390

Gopal A, Kant V, Gopalakrishnan A, Tandan SK, Kumar D (2014) Chitosan-based copper nanocomposite accelerates healing in excision wound model in rats. Eur J Pharmacol 731:8–19

George A, Raj DMA, Raj AD, Irudayaraj AA, Arumugam J, Senthilkumar M, Prabu HJ, Sundaram SJ, Al-Dhabi NA, Arasu MV, Maaza M, Kaviyarasu K (2020) Temperature effect on CuO nanoparticles: Antimicrobial activity towards bacterial strains. Surfaces Interfaces 21:100761

Hamzah, A. M. C., Yeo, C. C., Puah, S. M., Chua, K. H. and Chew, C. H (2019) *Staphylococcus aureus* Infections in Malaysia: a review of antimicrobial resistance and characteristics of the clinical isolates, 1990–2017. Antibiotics 8(128)

Hosseinzadeh R, Mohadjerani M, Mesgar S (2017) Green synthesis of copper oxide nanoparticles using aqueous extract of *Convolvulus percicus L.* as reusable catalysts in cross- coupling reactions and their antibacterial activity. IET Nanobiotechnol 11(6):725–730

Han G, Ceilley R (2017) Chronic wound healing: a review of current management and treatments. Adv Ther 34:599–610

Harun NH, Mydin RBSMN, Sreekantan S et al (2021) In vitro biointeraction responses and hemocompatibility of nano-based linear low-density polyethylene polymer embedded with heterogeneous TiO_2/ZnO nanocomposites for biomedical applications. J Biomater Sci Polym Ed 32(10):1301–1311

Hublikar LV, Ganachari SV, Raghavendra N, Banapurmath NR, Patil VB, Yunus Khan TM, Badruddin IA (2021a) Biogenesis of Silver Nanoparticles and Its Multifunctional Anti-Corrosion and Anticancer Studies. Coatings 11:1215

Hublikar LV, Ganachari SV, Raghavendra N, Patil VB, Banapurmath NR (2021b) Green synthesis silver nanoparticles via Eichhornia Crassipes leaves extract and their applications. Current Res Green Sustain Chem 4:100212

Hamid A, Haq S, Ur Rehman S et al (2021) Calcination temperature-driven antibacterial and antioxidant activities of *fumaria indica* mediated copper oxide nanoparticles: characterization. Chem Pap 75:4189–4198

Ijaz F, Shahid S, Khan SA, Ahmad W, Zaman S (2017) Green synthesis of copper oxide nanoparticles using *Abutilon indicum* leaf extract: antimicrobial, antioxidant and photocatalytic dye degradation activities. Trop J Pharm Res 16(4):743–753

Jayakumar S, Baskaran N, Arumugam R, Sathiskumar S, Pugazhenthi M (2018) Herbal medicine as a live practice for treating livestock ailments by indigenous people: A case study from the Konar community of Tamil Nadu. S Afr J Bot 118:23–32

Jadhav MS, Kulkarni S, Raikar P, Barretto DA, Vootla SK, Raikar US (2017) Green Biosynthesis of CuO & Ag-CuO nanoparticles from *Malus Domestica* leaf extract and evaluation of antibacterial, antioxidant. DNA Cleav Activit New J Chem 42:204–213

Janowska A, Dini V, Oranges T, Iannone M, Loggini B, Romanelli M (2019) Atypical ulcers: diagnosis and management. Clin Interv Aging 14:2137–2143

Jiao Z, Zhou G, Zhang H, Shen Y, Zhang X, Li J, Gao X (2018) Effect of calcination temperature on catalytic performance of CeCu oxide in removal of quinoline by wet hydrogen peroxide oxidation from water. J Braz Chem Soc 29(11):2233–2243

Kannan RRR, Stirk WA, Van Staden J (2013) Synthesis of silver nanoparticles using the seaweed *Codium capitatum* P.C. Silva (Chlorophyceae). S Afr J Bot 86:1–4

Kumar PPNV, Shameem U, Kollu P, Kalyani RL, Pammi SVN (2015) Green synthesis of copper oxide nanoparticles using *Aloe vera* leaf extract and its antibacterial activity against fish bacterial pathogens. BioNanoScience 5:135–139

Kumari P, Panda PK, Jha E, Kumari K, Nisha K, Mallick MA, Verma SK (2017) Mechanistic insight to ROS and apoptosis regulated cytotoxicity inferred by green synthesized CuO nanoparticles from *Calotropis gigantea* to Embryonic Zebrafish. Sci Rep 7:16284

Khan TM, Mateen AU (2018) Synthesis of CuO Nanoparticles by using Leaf Extracts of *Melia azedarach* and *Morus nigra* and their Antibacterial Activity. J Innov Sci 4(2):120

Kannan S, Solomon A, Krishnamoorthy G et al (2021) Liposome encapsulated surfactant abetted copper nanoparticles alleviates biofilm mediated virulence in pathogenic *Pseudomonas aeruginosa* and MRSA. Sci Rep 11:1102

Lediga ME, Malatjie TS, Olivier DK, Ndinteh DT, van Vuuren SF (2018) Biosynthesis and characterisation of antimicrobial silver nanoparticles from a selection of fever-reducing medicinal plants of South Africa. S Afr J Bot 119:172–180

Luna I, Hilary L, Chowdhury A, Gafur M, Khan N, Khan R (2015) Preparation and characterization of copper oxide nanoparticles synthesized via chemical precipitation method. Open Access Library J 2:1–8

Laha D, Pramanik A, Laskar A, Jana M, Pramanik P, Karmakar P (2014) Shape-dependent bactericidal activity of copper oxide nanoparticle mediated by DNA and membrane damage. Mater Res Bull 59:185–191

Lee SB, Ko EH, Park JY, Oh JM (2021) mixed metal oxide by calcination of layered double hydroxide: parameters affecting specific surface area. Nanomaterials (basel) 11(5):1153

Mtambo SE, Krishna SBN, Sershen GP (2019) Physico-chemical, antimicrobial and anticancer properties of silver nanoparticles synthesised from organ-specific extracts of *Bidens pilosa* L. S Afr J Bot 126:196–206

Maria A, Vincent MV, Mookkaiah R, Subramani R, Nadesan K (2020) Catharanthus roseus leaf extract mediated facile green synthesis of copper oxide nanoparticles and its photocatalytic activity. Chem Methodol 4:424–436

Mydin RBSMN, Zahidi INM, Ishak NN, Ghazali NSSN, Moshawih S, Siddiquee S (2018) Potential of calcium carbonate nanoparticles for therapeutic applications. Malaysian J Med Health Sci 14(SUPP1):201–206

Marquis G, Ramasamy B, Banwarilal S, Munusamy AP (2015) Evaluation of antibacterial activity of plant mediated CaO nanoparticles using *cissus quadrangularis* extract. J Photochem Photobiol 155:28–33

Mongkholrattanasit R, Krystufek J, Wiener J, Studnickova J (2011) Natural dye from *Eucalyptus* leaves and application for wool fabric dyeing by using padding techniques. Natural Dyes. IntechOpen 4

Majeed S, Danish M, Mohamad Ibrahim MN et al (2021) Bacteria mediated synthesis of iron oxide nanoparticles and their antibacterial, antioxidant, cytocompatibility properties. J Cluster Sci 32:1083–1094

Mahamuni PP, Patil PM, Dhanavade MJ, Badiger MV, Shadija PG, Lokhande AC, Bohara RA (2019) Synthesis and characterization of zinc oxide nanoparticles by using polyol chemistry for their antimicrobial and antibiofilm activity. Biochem Biophys Rep 17:71–80

Nussbaum SR, Carter MJ, Fife CE, DaVanzo J, Haught R, Nusgart M, Cartwright D (2018) An economic evaluation of the impact, cost, and medicare policy implications of chronic nonhealing wounds. Value Health 21(1):27–32

Hanina NH, A. W., Intan, N. S., Syafinaz, A. N., Zalinah, A., Lailatul Akmar, M. N., Devnani, A.S. (2015) Clinical presentation and microorganisms sensitivity profile for diabetic foot ulcers: a pilot study. Med J Malaysia 70(3):182–187 (**PMID: 26248782**)

Naika HR, Lingaraju K, Manjunath K, Kumar D, Nagaraju G, Suresh D, Nagabhushana H, H, (2015) Green synthesis of CuO nanoparticles using *Gloriosa superba L.* extract and their antibacterial activity. J Taibah Univ Sci 9:7–12

Narasaiah P, Mandal BK, Sarada NC (2017) Biosynthesis of Copper oxide nanoparticles from *Drypetes sepiaria* leaf extract and their catalytic activity to dye degradation. IOP Conf Ser Mater Sci Eng 263:022012

Naqvi QuA, Kanwal A, Qaseem S et al (2019) Size-dependent inhibition of bacterial growth by chemically engineered spherical ZnO nanoparticles. J Biol Phys 45:147–159

Pacios O, Blasco L, Bleriot I, Fernandez-Garcia L, Bardanca MG, Ambroa A, Lopez M, Bou G, Tomas M (2020) Strategies to combat multidrug-resistant and persistent infectious diseases. Antibiotics 9(65)

Prasad KS, Patra A, Shruthi G, ChandanS (2017) Aqueous extract of *Saraca indica* leaves in the synthesis of copper oxide nanoparticles: finding a way towards going green. J Nanotechnol 7502610

Qamar H, Rehman S, Chauhan DK, Tiwari AK, Upmanyu V (2020) Green synthesis, characterization and antimicrobial activity of copper oxide nanomaterial derived from *Momordica charantia*. Int J Nanomed 15:2541–2553

Ravele MP, Oyewo OA, Ramaila S, Mavuru L, Onwudiwe DC (2022) Facile synthesis of copper oxide nanoparticles and their applications in the photocatalytic degradation of acyclovir. Results Eng 14:100479

September J, Geffen L, Manning K, Naicker P, Faro C, Mendelson M, Wasserman S (2019) Colonisation with pathogenic drug-resistant bacteria and Clostridioides difficile among residents of residential care facilities in Cape Town, South Africa: a cross-sectional prevalence study. Antimicrob Resist Infect Control 8:180

Sharma JK, Akhtar M, S., Ameen, S., Srivastava, P. and Singh, G, (2015) Green synthesis of CuO nanoparticles with leaf extract of *Calotropis gigantea* and its dye-sensitized solar cells applications. J Alloy Compd 632:321–325

Sorbiun M, Mehr ES, Ramazani A, Fardood ST (2018) Green Synthesis of Zinc Oxide and Copper Oxide Nanoparticles Using Aqueous Extract of Oak Fruit Hull (Jaft) and Comparing Their Photocatalytic Degradation of Basic Violet 3. Int J Environ Res 12:29–37

Sharma D, Thakur N, Vashistt J, Bisht GS (2018) Antibacterial evaluation of cuprous oxide nanoparticles synthesized using leaf extract of *Callistemon viminalis*. Indian J Pharm Educ Res 52(3)

Singh J, Kumar V, Kim K, Rawat M (2019) Biogenic synthesis of copper oxide nanoparticles using plant extract and its prodigious potential for photocatalytic degradation of dyes. Environ Res 177:108569

Sarkar J, Chakraborty N, Chatterjee A, Bhattacharjee A, Dasgupta D, Acharya K (2020) Green synthesized copper oxide nanoparticles ameliorate defence and antioxidant enzymes in *Lens culinaris*. Nanomaterials 10(312)

Santhoshkumar J, Shanmugam V (2020) Green synthesis of copper oxide nanoparticles from *Magnolia Champaca* floral extract and its antioxidant and toxicity assay using Danio Rerio. Int J Recent Technol Eng 8(5):5444

Sukumar S, Rudrasenan A, Nambiar DP (2020) Green-synthesized rice-shaped copper oxide nanoparticles using *Caesalpinia bonducella* seed extract and their applications. ACS Omega 5:1040–1051

Saravanan S, Sivasankar T (2016) Effect of ultrasound power and calcination temperature on the sonochemical synthesis of copper oxide nanoparticles for textile dyes treatment. Environ Prog Sustain Energy 35(3):669

Siddiqi KS, Husen A (2020) Current status of plant metabolite-based fabrication of copper/copper oxide nanoparticles and their applications: a review. Biomater Res 24 (11)

Son Y, Park S (2018) Green preparation and characterization of graphene oxide/carbon nanotubes loaded carboxymethyl cellulose nanocomposites. Sci Rep 8:17601

Sung T, Wang Y, Liu K, Chou C, Lai P, Hsieh C (2020) Pholiota nameko polysaccharides promotes cell proliferation and migration and reduces ROS content in H_2O_2-induced L929 cells. Antioxidants 9(65)

Sirelkhatim A, Mahmud S, Seeni A et al (2016) Preferential cytotoxicity of ZnO nanoparticle towards cervical cancer cells induced by ROS-mediated apoptosis and cell cycle arrest for cancer therapy. J Nanopart Res 18(8):219

Shi, L., Tang, P., Zhang, W., Zhao, Y., Zhang, L. and Zhang, H (2017) Green synthesis of CuO nanoparticles using *Cassia auriculata* leaf extract and in vitro evaluation of their biocompatibility with rheumatoid arthritis macrophages (RAW 264.7). Trop J Pharm Res 16(1):185–192

Sachett A, Gallas-Lopes M, Conterato GMM, Herrmann AP,Piato A (2021) Antioxidant activity by DPPH assay: in vitro protocol

Thakur BK, Kumar A, Kumar D (2019) Green synthesis of titanium dioxide nanoparticles using *Azadirachta indica* leaf extract and evaluation of their antibacterial activity. S Afr J Bot 124:223–227

Tu HL (2019) Biosynthesis, Characterization and photocatalytic activity of copper/copper oxide nanoparticles produced using aqueous extract of *Lemongrass* Leaf. Comp Mater 3(1):30–35

Tavakoli S, Kharaziha M, Ahmadi S (2019) Green synthesis and morphology dependent antibacterial activity of copper oxide nanoparticles. J Nanostruct 9(1):163–171

Uckay I, Aragon-Sanchez J, Lew D, Lipsky BA (2015) Diabetic Foot Infections: What have we learned in the last 30 years? Int J Infect Dis 40:81–91

Umar A, Kumar R, Kumar G, Algarni H, Kim SH (2015) Effect of annealing temperature on the properties and photocatalytic efficiencies of ZnO nanoparticles. J Alloy Compd 648:46–52

Velsankar K, Vinothini V, Sudhahar S, Kumar MK, Mohandoss S (2020) Green synthesis of CuO nanoparticles via *Plectranthus amboinicus* leaves extract with its characterization on structural, morphological, and biological properties. Appl Nanosci 10:3953–3971

Wang M, Wei H, Zhao Y, Shang L, Di L, Lyu C, Liu J (2019) Analysis of multidrug-resistant bacteria in 3223 patients with hospital-acquired infections (HAI) from a tertiary general hospital in China. Bosn J Basic Med Sci 19(1):86–93

Wong SY, Manikam R, Muniandy S (2015) Prevalence and antibiotic susceptibility of bacteria from acute and chronic wounds in Malaysian subjects. J Infect Dev Ctries 9(9):936–944

Xu P, Chen L, Wang Y (2019) Effect of storage time on antioxidant activity and inhibition on α-Amylase and α-Glucosidase of white tea. Food Sci Nutr 7:636–644. https://doi.org/10.1002/fsn3.899

Yu J, Yu H, Cheng B, Zhao X, Yu JC, Ho W (2003) The Effect of calcination temperature on the surface microstructure and photocatalytic activity of TiO_2 thin films prepared by liquid phase deposition. J Phys Chem B 107:13871–13879

Yang Z, Hao X, Chen S, Ma Z, Wang W, Wang C, Yue L, Sun H, Shao Q, Murugadoss V, Guo Z (2018a) Long-term antibacterial stable reduced graphene oxide nanocomposites loaded with cuprous oxide nanoparticles. J Coll Interface Sci 533:13–23

Yang X, Zhang L, Jiang X (2018b) Aminosaccharide–gold nanoparticle assemblies as narrow-spectrum antibiotics against methicillin-resistant *Staphylococcus aureus*. Nano Res 11:6237–6243

Yin Y, Lin Q, Sun H et al (2012) Cytotoxic effects of ZnO hierarchical architectures on RSC96 Schwann cells. Nanoscale Res Lett 7(1):439

Zayyoun N, Bahmad L, Laânab L et al (2016) The effect of pH on the synthesis of stable Cu_2O/CuO nanoparticles by sol–gel method in a glycolic medium. Appl Phys A 122:488